NTU-90: A High Angular Resolution Brain Atlas Constructed by Q-Space Diffeomorphic Reconstruction

Fang-Cheng Yeh[1], and Wen-Yih Isaac Tseng[2,3,*]

[1]Department of Biomedical Engineering, Carnegie Mellon University, Pennsylvania, USA;

[2]Department of Medical Imaging, National Taiwan University Hospital, Taipei, Taiwan;

[3]Center for Optoelectronic Biomedicine, National Taiwan University College of Medicine, Taipei, Taiwan

*Correspondence to:

Wen-Yih Isaac Tseng, M.D., Ph.D.,

Center for Optoelectronic Biomedicine

National Taiwan University College of Medicine

No. 1, Sec 1, Jen-Ai Rd., Taipei, Taiwan 100

Tel: +886-2-2312-3456 ext. 88758

Fax: +886-2-2392-6922

Email: wytseng@ntu.edu.tw

ABSTRACT

We present a high angular resolution brain atlas constructed by averaging 90 diffusion spectrum imaging (DSI) datasets in the ICBM-152 space. The spatial normalization of the diffusion information was conducted by a novel q-space diffeomorphic reconstruction method, which reconstructed the spin distribution function (SDF) in the ICBM-152 space from the diffusion MR signals. The performance of this method was examined by a simulation study modeling nonlinear transformation. The result showed that the reconstructed SDFs can resolve crossing fibers and that the accumulated quantitative anisotropy can reveal the relative ratio of the fiber populations. In the *in vivo* study, the SDF of the constructed atlas was shown to resolve crossing fiber orientations. Further, fiber tracking showed that the atlas can be used to present the pathways of fiber bundles, and the termination locations of the fibers can provide anatomical localization of the connected cortical regions. This high angular resolution brain atlas may facilitate future connectome research on the complex structure of the human brain.

Key words: diffusion MRI atlas, q-space diffeomorphic reconstruction, quantitative anisotropy.

INTRODUCTION

Diffusion MRI is a noninvasive imaging method to reveal the underlying white matter structure of the human brain (Merboldt et al., 1992; Moseley et al., 1993). By using the diffusion tensor model, diffusion MRI can be used to reconstruct diffusion tensor imaging (DTI)(Basser et al., 1994), which has been used to study the fiber orientations and the quantitative measurement of the diffusion characteristics (Basser and Pierpaoli, 1996; Pierpaoli and Basser, 1996; Pierpaoli et al., 1996). The axonal connections in the human brain can also be assessed by applying streamline fiber tracking on DTI data (Basser et al., 2000; Conturo et al., 1999; Mori et al., 1999). The application of diffusion MRI has been extended to group studies, which aim to construct an atlas by linearly or nonlinearly transforming individual brains to a template space. This approach offers ensemble information about the human brain and may play an important role in the study of brain connectome (Williams, 2010).

To provide reliable ensemble information, an atlas needs to resolve accurate principal fiber directions and to offer consistent results of the quantitative analysis. To satisfy these purposes, studies have been conducted using affine transform (Jones et al., 2002; Mori et al., 2008; Muller et al., 2007) or nonlinear transformation (Ardekani and Sinha, 2006; Goodlett et al., 2006; Park et al., 2003; Peng et al., 2009; Van Hecke et al., 2008; Xu et al., 2003; Zhang et al., 2006; Zhang et al., 2011). Although these templates have provided various solutions to construct an atlas, they are all based on DTI, which is known to have the following limitations: difficulty in resolving crossing fibers (Alexander et al., 2002; Tuch et al., 2002) and the partial volume effect, which leads to inaccurate estimation of the anisotropy index in the fiber crossing regions (Alexander et al., 2001; Barrick and Clark, 2004; Oouchi et al., 2007).

The crossing fiber limitation could be solved by using an orientation distribution function (ODF) to characterize the diffusion distribution or fiber populations. The diffusion images can be acquired by using a single-shell diffusion sampling scheme, which is also known as high angular resolution diffusion image (HARDI)(Tuch et al., 2002) acquisition, or by using a grid sampling scheme, which is known as diffusion spectrum imaging (DSI)(Wedeen et al., 2005) acquisition. Model-free reconstruction methods include q-ball imaging (QBI)(Tuch, 2004) and DSI, which model diffusion distribution by a probability based approach and calculate diffusion ODFs. Deconvolution methods include spherical deconvolution (Tournier et al., 2004), which calculates the volume fraction of fiber populations and obtains the fiber orientation distribution (FOD). To further apply spatial transformation to these ODF-based methods, a recent study was proposed to obtain the transformed FOD from the high angular resolution diffusion image (HARDI) (Hong et al., 2009). However, this method is limited to linear transformation, and the transformed FOD

has not yet been shown to provide an anisotropic index for quantitative analysis.

In addition to the crossing fiber limitation, the partial volume problem is still under active research. Although fiber crossing can be resolved by using HARDI acquisition, one recent study showed that the generalized fractional anisotropy (GFA) offered by QBI is also vulnerable to the partial volume effect of crossing fibers (Fritzsche et al., 2010), indicating that studies using ODF to characterize diffusion distribution may also suffer from the partial volume effect. This result can be understood by the fact that the ODF of the diffusion distribution (e.g. diffusion ODF) or fibers volume fraction (e.g. FOD) are fractional values, not the actual amount of the diffusion spins. The partial occupation of crossing fibers or background diffusion will inevitably change the fractional values, leading to a consequence known as the partial volume effect. This problem is even more challenging when nonlinear transformation is applied to the ODF. The transformation may contain scaling and shearing that alters the fractional measurement of the diffusion spins and causes difficulties in transforming an ODF to the template space. To solve this problem, a possible solution is to use the spin distribution function (SDF), which presents the amount of the spins undergoing diffusion in different orientations. The SDF can be estimated by using generalized q-sampling imaging (GQI) (Yeh et al., 2010), with the expense of an additional spin density scan for calibration.

In this study, we aimed to construct a high angular resolution brain atlas in the ICBM-152 space using the SDF measurement. To obtain the SDFs in the ICBM-152 space (termed transformed SDF in the following texts, as opposed to the original SDF, which is the SDF obtained from GQI without transformation), we propose a novel method called q-space diffeomorphic reconstruction, which can calculate transformed SDFs in any given deformation field that satisfies diffeomorphism. This method can employ linear or non-linear registration, including registration based on diffusion images (Chiang et al., 2008; Hong et al., 2009; Yap et al., 2010; Yap et al., 2011) or registration based on structure images. The q-space diffeomorphic reconstruction aims to preserve fiber orientations so that these orientations can be used to conduct fiber tracking. Moreover, this method aims to satisfy the conservation of diffusion spins, and the transformed SDFs can be used to conduct quantitative analysis.

To demonstrate the performance of this method, we simulated a 90°-crossing phantom and applied nonlinear transformation that models scaling and rotation. The transformed SDFs were examined and compared with the original SDFs to examine their abilities to resolve crossing fibers and to provide quantitative analysis. Streamline fiber tracking was conducted to examine the fiber tracts generated from the resolved fiber orientations.

To construct a high angular resolution brain atlas, we collected a total of 90 DSI datasets, and SPM5 (Wellcome Trust Centre for Neuroimaging, London, UK) was used to obtain the nonlinear transformation that maps each subject space to the ICBM-152 space. The transformed SDFs in the ICBM-152 space were reconstructed using the q-space diffeomorphic reconstruction, and our NTU-90 atlas was constructed by averaging the transformed SDFs of these 90 DSI datasets. The averaged SDFs were examined to confirm the ability to resolve crossing fiber, and streamline fiber tracking was applied to present potential applications of the atlas in brain studies.

Materials and methods

Diffeomorphic mapping

Diffeomorphic mapping can be formulated as the following equation: $\varphi(\mathbf{r_s}) = \mathbf{r_t}$, where φ is the mapping function ($\varphi : R^3 \to R^3$), $\mathbf{r_s}$ is the coordinates in the subject space, and $\mathbf{r_t}$ is the coordinates in the template space (e.g. the ICBM-152 space). Diffeomorphic mapping satisfies two prerequisites: φ has an invert function φ^{-1}, and both φ and φ^{-1} are differentiable. In other words, for any point $\mathbf{r_s}$, there exists a corresponding point $\varphi(\mathbf{r}_s)$ in the template space, and the Jacobian matrix $J_\varphi(\mathbf{r_s})$ can be evaluated at $\mathbf{r_s}$. This mapping approach provides a more general model for spatial transformation. For example, it can be used to model linear transformation: $\varphi(\mathbf{r_s}) = \mathbf{A}\mathbf{r_s} + \mathbf{t}$, where $\mathbf{A}$ is a 3-by-3 matrix and $\mathbf{t}$ is the translocation vector, or to model nonlinear mapping: $\varphi(\mathbf{r_s}) = \mathbf{r_s} + \cos(2\pi\mathbf{r_s} / R)$, where R is a length constant.

Spin conservation model

To obtain the transformed SDF, we introduce the concept of "conservation of diffusion spins," which ensures that the amount of the diffusion spins is conserved in the diffeomorphic mapping. To formulate this concept, we model the diffusion pattern in the subject space in terms of a density function $Q_s(\mathbf{r}_s, \mathbf{r}_s')$, which represents the number of the spins that move from coordinates $\mathbf{r}_s$ to coordinates $\mathbf{r}_s'$ in a specific diffusion time, and similarly, we model the corresponding density function in the template space as $Q_t(\mathbf{r}_t, \mathbf{r}_t')$, where $\varphi(\mathbf{r_s}) = \mathbf{r_t}$ and $\varphi(\mathbf{r_s}') = \mathbf{r_t}'$. With these notations, we model the conservation of the diffusion spins as follows:

$$Q_s(\mathbf{r}_s, \mathbf{r}_s')d\mathbf{r}_s = Q_t(\mathbf{r}_t, \mathbf{r}_t')d\mathbf{r}_t \qquad (1)$$

where $d\mathbf{r}_s$ and $d\mathbf{r}_t$ are differential volume elements at $\mathbf{r}_s$ and $\mathbf{r}_t$, respectively. Since the ratio of the diffusion displacement to the size of an image voxel in the combined k-space and q-space imaging is around 0.01 (Callaghan, 1993), we can assume that the diffusion displacement is

negligibly small in our spin conservation model. Thus the Jacobian matrix $J_{\varphi^{-1}}(\mathbf{r}_t)$ can be viewed as a constant value when the spins move from $\mathbf{r}_t$ to $\mathbf{r}_t'$, (i.e. $J_{\varphi^{-1}}(\mathbf{r}_t) \approx J_{\varphi^{-1}}(\mathbf{r}_t')$). This allows us to replace $d\mathbf{r}_s / d\mathbf{r}_t$ by the Jacobian determinant, $\left|J_{\varphi^{-1}}(\mathbf{r}_t)\right|$, and derive the following equation:

$$Q_s(\mathbf{r}_s, \mathbf{r}_s') = Q_t(\mathbf{r}_t, \mathbf{r}_t')\left|J_{\varphi^{-1}}(\mathbf{r}_t)\right|^{-1} \quad (2)$$

where $\left|J_{\varphi^{-1}}(\mathbf{r}_t)\right|^{-1}$ is the inverse of the Jacobian determinant of φ^{-1} at $\mathbf{r}_t$, and the subscript φ^{-1} denotes the inverse function of the diffeomorphic mapping φ. The spin conservation model can be further incorporated into the SDF, as described in the following section.

Spin distribution function

SDF is defined as the amount of the spins that undergo diffusion in different orientations (Yeh et al., 2010). By using the density function $Q_s(\mathbf{r}_s, \mathbf{r}_s')$ defined in the previous section, we can calculate the original SDF in the subject space as follows.

$$\psi_s(\mathbf{r}_s, \mathbf{u}) = \int_0^L Q_s(\mathbf{r}_s, \mathbf{r}_s + r\mathbf{u})dr \quad (3)$$

where r is the displacement variable that ranges from 0 to the diffusion sampling length L, and $\mathbf{u}$ is the sampling direction of the SDF. The transformed SDF in the template space, however, has to consider the scaling effect on displacement variable r due to the diffeomorphic mapping. Since a unit distance in the template space may not be equal to the same distance in the subject space, we calculate the SDF in the template space as follows:

$$\psi_t(\mathbf{r}_t, \mathbf{v}) = \int_0^L Q_t\left(\mathbf{r}_t, \mathbf{r}_t + \left\|J_{\varphi^{-1}}(\mathbf{r}_t)\mathbf{v}\right\|^{-1} r\mathbf{v}\right)dr \quad (4)$$

where $\left\| J_{\varphi^{-1}}(\mathbf{r}_t)\mathbf{v} \right\|$ is the vector norm of the transformed vector $J_{\varphi^{-1}}(\mathbf{r}_t)\mathbf{v}$. The additional term, $\left\| J_{\varphi^{-1}}(\mathbf{r}_t)\mathbf{v} \right\|^{-1}$, is added to cancel the scaling effect of the diffeomorphic mapping because the unit distance at $\mathbf{r}_t + r\mathbf{v}$ is scaled by $\left\| J_{\varphi^{-1}}(\mathbf{r}_t + r\mathbf{v})\mathbf{v} \right\|$, which can be approximated by $\left\| J_{\varphi^{-1}}(\mathbf{r}_t)\mathbf{v} \right\|$. Incorporating the spin conservation model stated in Eq. 2 into Eq. 4, we reformulated the SDF calculation in the template space as follows:

$$\psi_t(\mathbf{r}_t, \mathbf{v}) = \int_0^L Q_s\left(\varphi^{-1}(\mathbf{r}_t), \varphi^{-1}\left(\mathbf{r}_t + \left\| J_{\varphi^{-1}}(\mathbf{r}_t)\mathbf{v} \right\|^{-1} r\mathbf{v} \right) \right) \left| J_{\varphi^{-1}}(\mathbf{r}_t) \right| dr \qquad (5)$$

The term $\varphi^{-1}\left(\mathbf{r}_t + \left\| J_{\varphi^{-1}}(\mathbf{r}_t)\mathbf{v} \right\|^{-1} r\mathbf{v} \right)$ can be approximated by its Taylor expansion, $\varphi^{-1}(\mathbf{r}_t) + rJ_{\varphi^{-1}}(\mathbf{r}_t)\mathbf{v} \Big/ \left\| J_{\varphi^{-1}}(\mathbf{r}_t)\mathbf{v} \right\|$. The error of this approximation can be estimated by the first remainder of the Taylor expansion, whose vector norm is in proportion to $\frac{1}{2}\left(r \Big/ \left\| J_{\varphi^{-1}}(\mathbf{r}_t)\mathbf{v} \right\| \right)^2$, indicating that the error is at a scale of r^2. In practice, this error can be ignored, for we assume that the diffusion displacement r is sufficiently smaller than the image resolution in our spin conservation model. By using this approximation, the following relation between ψ_t and ψ_s can be derived:

$$\psi_t(\mathbf{r}_t, \mathbf{v}) = \left| J_{\varphi^{-1}}(\mathbf{r}_t) \right| \psi_s\left(\varphi^{-1}(\mathbf{r}_t), \frac{J_{\varphi^{-1}}(\mathbf{r}_t)\mathbf{v}}{\left\| J_{\varphi^{-1}}(\mathbf{r}_t)\mathbf{v} \right\|} \right) \qquad (6)$$

To further incorporate the Eq. 6 into the q-space reconstruction, we make use of the generalized q-sampling reconstruction method (Yeh et al., 2010), which formulates the relation between the original SDF and diffusion MR signals as the following equation:

$$\psi_s(\mathbf{r}_s, \mathbf{u}) = A\sum_i W_i(\mathbf{r}_s) \mathrm{sinc}\left(\sigma\sqrt{6Db_i} < \mathbf{g}_i, \mathbf{u} > \right) \qquad (7)$$

where A is the constant term for the SDF quadrature, and i iterates through all diffusion

acquisitions. W_i ($\mathbf{r_s}$) is the diffusion MR signal at $\mathbf{r_s}$ acquired by b-value=b_i and diffusion gradient direction=$\mathbf{g}_i$. σ is the diffusion length ratio that controls the covering percentage of the diffusion spins (e.g. σ = 1.25 covers more than 80% of the diffusion spins). *D* is the diffusivity of the diffusion spins, and $<\mathbf{g}_i, \mathbf{u}>$ the inner product of the diffusion gradient direction and ODF sampling direction (both are unit vectors). Combining Eq. 6, and 7, the equation for our q-space diffeomorphic reconstruction can be derived as follows:

$$\psi_t(\mathbf{r}_t, \mathbf{v}) = \left|J_{\varphi^{-1}}(\mathbf{r}_t)\right| A \sum_i W_i\left(\varphi^{-1}(\mathbf{r}_t)\right) \mathrm{sinc}\left(\sigma\sqrt{6Db_i} < \mathbf{g}_i, \frac{J_{\varphi^{-1}}(\mathbf{r}_t)\mathbf{v}}{\left\|J_{\varphi^{-1}}(\mathbf{r}_t)\mathbf{v}\right\|} >\right) \qquad (8)$$

Equation 8 is the reconstruction equation for our q-space diffeomorphic reconstruction method, which directly calculates the transformed SDF in the template space from the diffusion MR signals W_i. In this equation, the numerical estimations include 1) the estimation of $W_i\left(\varphi^{-1}(\mathbf{r}_t)\right)$, which can be implemented by trilinear interpolation; 2) the transformed sampling vector, $J_{\varphi^{-1}}(\mathbf{r}_t)\mathbf{v}$, which can be estimated by $\frac{\varphi^{-1}(\mathbf{r}_t + \varepsilon\mathbf{v}) - \varphi^{-1}(\mathbf{r}_t - \varepsilon\mathbf{v})}{2\varepsilon}$ if an analytical form is not available; 3) the Jacobian determinant $\left|J_{\varphi^{-1}}(\mathbf{r}_t)\right|$, which can be calculated analytically or estimated by numerical approximation.

Quantitative analysis

The diffusion characteristics of a fiber population can be analyzed by using quantitative anisotropy (QA) (Yeh et al., 2010), which is defined as the amount of the spins that undergo diffusion along the fiber orientation:

$$QA(\mathbf{r}, \hat{\mathbf{a}}) = Z_0\left(\psi(\mathbf{r}, \hat{\mathbf{a}}) - I(\psi(\mathbf{r}))\right) \qquad (9)$$

where $\hat{\mathbf{a}}$ is the orientation of the fiber defined by the local maximum of the SDF, and $I(\psi(\mathbf{r}))$ is the background isotropic component, which can be approximated by the minimum value of the SDF, i.e. $\min_{\mathbf{u}}(\psi(\mathbf{r}, \mathbf{u}))$. Z_0 is a constant that scales the amount of diffusion spins with respect to 1 mm^3 free water diffusion, and Z_0 satisfies $Z_0 I(\psi_0) = 1$, where ψ_0 is a SDF estimated from a 1 mm^3 free water diffusion voxel. If ψ_0 is measured from a voxel having a larger volume, e.g. 2 mm^3, we may calibrate Z_0 by $Z_0 I(\psi_0) = 2$, assuming that the linearity relation holds. One should

note that the calibration needs to be conducted in the subject space, since the volume of the free water diffusion we mentioned here is in the subject space. The estimation of Z_0 can be made by considering cerebrospinal fluid (CSF) as free water diffusion and using voxels in CSF to calibrate Z_0. A more accurate approach can be conducted by including a free water tube in the scanner as a calibration sample. By calibrating the Z_0 constant, QA has a unit in mm^3, which represents the equivalent volume of diffusion spins that diffuse in the fiber orientation $\hat{\mathbf{a}}$. For example, $QA(\mathbf{r},\hat{\mathbf{a}})=0.2$ mm^3 means that the amount of the spins moving in orientation $\hat{\mathbf{a}}$ is equivalent to 0.2 mm^3 within a unit voxel at $\mathbf{r}$. If the fiber spans multiple voxels, we may also calculate the accumulated QA as follows:

$$\int_R QA(\mathbf{r},\hat{\mathbf{a}}(\mathbf{r}))d\mathbf{r} \qquad (10)$$

where R is the region occupied by the fiber and $\hat{\mathbf{a}}(\mathbf{r})$ is the fiber orientation at coordinate $\mathbf{r}$.

Atlas construction

An SDF atlas can be constructed by averaging the transformed SDFs of each subject:

$$\overline{\psi}_t(\mathbf{r}_t,\hat{\mathbf{u}}) = \frac{1}{n}\sum_{i=1}^{n}\psi_{t,i}(\mathbf{r}_t,\hat{\mathbf{u}}) \qquad (11)$$

where i denotes the ith subject, n is the total number of the subjects, and $\psi_{t,i}$ is the transformed SDF of the ith subject. One should note that this direct averaging approach is feasible because the transformed SDF is a quantity-based measure. For measures based on fractional values such as probability or volume fraction, weighted averaging should be used to consider the difference in spin quantity between subjects.

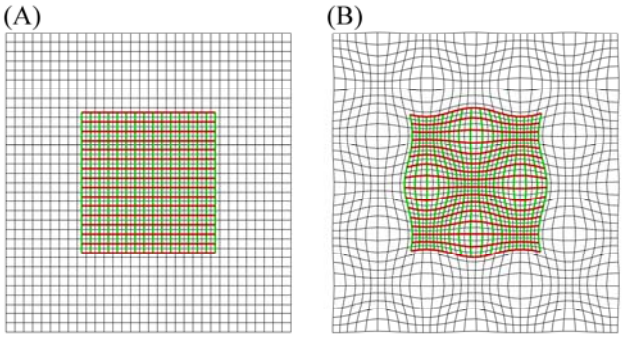

Fig. 1 (A) The original field of the simulated crossing fibers. (B) The transformation field of the diffeomorphism applied to the crossing fibers. The green lines represent the vertical fibers, and the red lines represent the horizontal fibers. The diffeomorphism models nonlinear transformation that includes scaling and rotation.

Simulation study

To examine the performance of the q-space diffeomorphic reconstruction, we simulated 90° crossing fibers in a 128 mm × 128 mm × 5 mm space with each voxel having 1 mm isotropic resolution. The crossing fibers, sized 64 mm × 64 mm × 5 mm, contained two fiber populations crossed at a right angle and were placed in the center of the space, as shown in Fig.1 (a). For each simulation voxel, the diffusion MRI signals were simulated by using a mixed Gaussian model that consists of two fiber populations (Alexander et al., 2002; Tuch et al., 2002).

$$\mathrm{S}(b,\hat{\mathbf{b}}) = S(0)\, f_1 \exp\left(-b\hat{\mathbf{b}}^{\mathrm{T}}\mathrm{D}_1\hat{\mathbf{b}}\right) + S(0)\, f_2 \exp\left(-b\hat{\mathbf{b}}^{\mathrm{T}}\mathrm{D}_2\hat{\mathbf{b}}\right) \qquad (12)$$

where b and $\hat{\mathbf{b}}$ are the b-value and the diffusion gradient direction, respectively. The fiber population ratio between the horizontal and vertical fibers was set to 3:2, resulting in f_1 =0.6, and f_2 =0.4. D_1 and D_2 are the diffusion tensor matrices, having a fractional anisotropy (FA) value of 0.67. This FA value was determined according to the *in vivo* FA value of the genu and splenium of corpus callosum (Bhagat et al., 2007). The D_1 tensor is oriented in the horizontal direction, and the D_2 tensor is oriented in the vertical direction. Mean diffusivity was set to 0.5 x 10^{-3} mm^2/s. The signal behavior in the background follows a simple exponential decay that simulates free water diffusion. The images were simulated under b0-SNR = 100 with Rician noise (Gudbjartsson and Patz, 1995) added. A 203-point grid sampling scheme with a maximum b-value of 6000 s/mm2 was used to generate the MR signals. The grid sampling points were obtained by iterating the integers q_x, q_y, and q_z and satisfying that $q_x^2 + q_y^2 + q_z^2 \le 13$, a setting that is according to the optimum DSI sampling scheme recommended by Kuo et al. (2008).

To fully exploit the diffeomorphic features, we devised a nonlinear transformation field φ, whose inverse function is defined as follows:

$$\varphi^{-1}\left(\begin{bmatrix} x \\ y \\ z \end{bmatrix}\right) = \begin{bmatrix} x + 2\cos(6\pi\, y/L)\sin(6\pi\, x/L) \\ y + 2\sin(6\pi\, y/L)\cos(6\pi\, x/L) \\ z \end{bmatrix} \qquad (13)$$

where L is the dimension of the space in the x and y directions (L=128 in this simulation). The analytics form of the Jacobian matrix is also available.

$$J_{\varphi^{-1}}\left(\begin{bmatrix} x \\ y \\ z \end{bmatrix}\right)=\begin{bmatrix} 1+12\pi\cos(6\pi\, y/L)\cos(6\pi\, x/L)/L & -12\pi\sin(6\pi\, y/L)\sin(6\pi\, x/L)/L & 0 \\ -12\pi\sin(6\pi\, y/L)\sin(6\pi\, x/L)/L & 1+12\pi\cos(6\pi\, y/L)\cos(6\pi\, x/L)/L & 0 \\ 0 & 0 & 1 \end{bmatrix} \quad (14)$$

The resulting deformation field φ is shown in Fig. 1(b). The crossing angles range from 57.27° to 90.00°. This range is within the resolution limit of DSI (Zhan and Yang, 2006); therefore, the failure to resolve the crossing angle can be totally attributed to our proposed reconstruction method. Moreover, the local stretch ratios (deformed length/original length) of the deformation field range from 0.77 to 1.42, whereas those of our in-house collected DSI dataset after normalization range from 0.84 to 1.10. Therefore, the deformation field used in our simulation can generate comparable distortion to examine our reconstruction method.

Our q-space diffeomorphic reconstruction method was applied to the simulated MR signals to obtained the transformed SDFs. The diffusion sampling length ratio (σ) was set to 1.25, as recommended by the GQI study, to cover more than 80% of the diffusion spins. The SDF had 642 sampling orientations generated from tessellating an icosahedron (8 divisions on each edge), resulting in angular resolution equal to 8.09°. For comparison, the original SDFs were obtained from the GQI reconstruction using the same setting (σ=1.25).

The fiber orientations were determined by the peak orientations of an SDF, and the angular error is defined as the inner angle between the resolved fiber orientation and the actual fiber geometry. The angular error of the transformed SDF was compared with the angular resolution of our ODF sampling (8.09°) to examine whether the angular error was significantly larger than the ODF sampling resolution. The modified streamline fiber tracking (Wedeen et al., 2008) was conducted using the fiber orientations defined by the transformed SDFs to examine whether the generated tractography could reveal the connections in the horizontal and vertical directions. The starting locations of the fiber tracts were randomly placed within the phantom region, and the initial direction was determined by the peak orientations of the SDFs. If an SDF had more than one peak orientation, the initial direction was randomly chosen from the resolved orientations. Trilinear interpolation was used to estimate the propagation direction. The step size was 0.5 mm (half of the spacing), and the maximum turning angle was 60°. The QA values were used to

determine the termination of the fiber, and a QA threshold of 0.1 mm^3 per voxel was chosen to include the minimum QA value of the fiber populations in the simulated phantom.

In addition to the fiber orientations, we also compared the QA values of the horizontal fibers with those of the vertical fibers. The accumulated QA of each fiber population was further calculated to examine whether it could reveal the population ratio between the horizontal and vertical fibers (f_1 =0.6, and f_2 =0.4). This analysis was conducted on both the original and transformed SDF to examine whether the analysis results from the two were consistent.

MRI acquisition

A total of 90 volunteers (45 males and 45 females) were included in this study. The subjects ranged in age from 18 to 60 years old. The mean ages of the male and female volunteers were 32.58 and 33.58 years old, respectively, with standard deviations of 12.96 and 12.26, respectively. The age difference was not statistically significant (p=0.7078, two-tail). The volunteers had no known history of neurological or mental disorder. The study was approved by the Research Ethics Committee at the National Taiwan University Hospital. Written informed consent was obtained from the participants.

The diffusion MR images were acquired on a 3T MRI scanner (Trio, Siemens, Erlangen, Germany) using an 8-channel head coil. The structure images was acquired by a T_2-weighted fast spin echo sequence with parameters TR/TE=5920/102 ms, and slice thickness of 3.0 mm, 256×256 acquisition matrix, and 25×25 cm field of view rendered in 35 axial slices. The diffusion images were acquired by using a pulse-gradient spin-echo diffusion EPI sequence with twice-refocused balanced echo (Reese et al., 2003). A total of 45 trans-axial slices were acquired to cover the whole brain. An isotropic spatial resolution of 3 mm was obtained in both in-plane and through-plane resolutions. The maximum diffusion sensitivity (b-max) was 6000 s/mm^2 and TR/TE was 9100/142 ms. A total of 203 grid sampling points were acquired as proposed by an optimization study (Kuo et al., 2008), resulting in a scanning time of 45 minutes.

The diffeomorphic mapping between each individual and the ICBM-152 template was obtained using SPM5 (Wellcome Trust Centre for Neuroimaging, London, UK). For each subject, the b0 image was linearly registered to the T_2-weighted image using mutual information as the cost function. The T_2-weighted image was then nonlinearly normalized to the ICBM-152 T_2 template with source smoothing = 8 mm, frequency cutoff = 25, iterations = 16, and voxel sizes = 2 mm×2 mm×2 mm. A total of 7×9×7=441 coefficients were obtained in the normalization process. The

overall diffeomorphic mapping was then obtained by combining the result of the linear registration and nonlinear normalization. The transformed SDFs were obtained by our q-space diffeomorphic reconstruction method with σ=1.25. The obtained SDFs of each subject were averaged to construct the NTU-90 brain atlas, resulting in a 2 mm×2 mm×2 mm high angular resolution diffusion atlas. The NTU-90 atlas can be downloaded from http://dsi-studio.labsolver.org.

The fiber tracking on the NTU-90 atlas was also conducted using the same tracking algorithm used in the phantom study. We selected arcuate fasciculus as the test example, since it is known to have superimposed crossing fibers that cannot be resolved by DTI, and its functional localization in the cerebral cortex is well-established. This allowed us to examine the accuracy of the tractography by correlating the fiber termination locations with the functional anatomy of language processing. The seeding region was selected manually using the interface provided by DSI Studio (http://dsi-studio.labsolver.org). An oval seeding region with a radius of 14 mm was manually placed at the supramarginal gyrus, and only the fibers passing in the anterior-posterior direction were selected. The step size was 1 mm, and the turning angle was 60°. QA values were used to determine the termination of the tracking algorithm. A QA threshold of 0.164 mm^3 per voxel was used based on the inspected QA values near the gray-white junction.

To compare the NTU-90 atlas with a DTI atlas, we conducted fiber tracking on the IIT2 template (Zhang et al., 2011), which has a spatial resolution of 1 mm. An identical tracking algorithm, seeding strategy, fiber selection direction, and parameters were used, except that the principal eigenvector of the tensor matrix was used as the fiber orientation and that the FA were used to determine the fiber termination. An FA threshold of 0.164 was used to obtain the same white matter coverage. The termination locations of the fiber tracts were examined by using the cortical surface rendered from the ICBM white matter atlas (Fonov et al., 2011).

RESULTS

Simulation

The analysis of the angular error showed that the average angular error of the horizontal fibers was 2.25° on the transformed SDFs, whereas that of the vertical fibers was 2.27°. These two errors are significantly smaller than the angular resolution of an ODF, which is 8.09° ($p < 0.001$). This result suggests that in our 90°-crossing simulation, the resolved fibers on the transformed SDFs achieved the angular resolution of our ODF sampling. This meets our aim that the transformed SDFs obtained from our q-space diffeomorphic reconstruction preserve the fiber orientations and can be used in fiber tracking.

The results of fiber tracking applied to the transformed SDF are shown in Fig. 2. The horizontal fiber (red) and vertical fibers (green) are presented separately for ease of viewing. The horizontal and vertical fiber tracts show continuous tracts, and the tracts are consistent with our simulation and deformation setting shown in Fig. 1. This result suggests that fiber tracking can be applied to the fiber orientations resolved from the transformed SDFs to tract the fiber pathways and to reveal the connection pattern between connected regions.

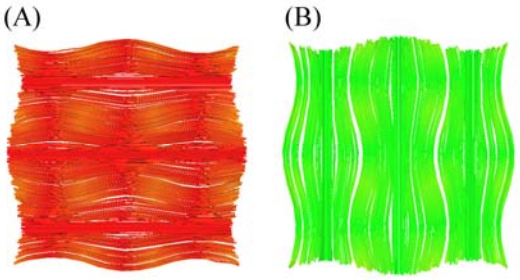

Fig. 2 The fiber tracking results of the (A) horizontal fibers and (B) vertical fibers. The fiber tracking is based on the fiber orientations obtained from the q-space diffeomorphic reconstruction. The fiber tracts show continuous routes that are consistent with the deformation field shown in Fig. 1(B), suggesting that the fiber tracking is still applicable to the fiber orientations obtained from the q-space diffeomorphic reconstruction.

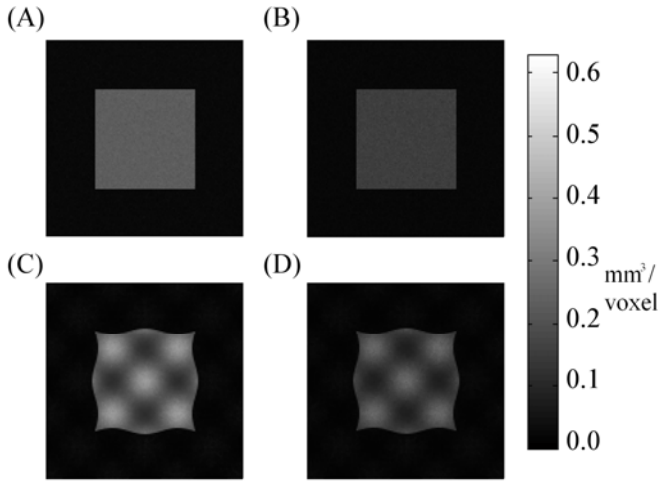

Fig. 3 (A) The quantitative anisotropy (QA) mapping of the horizontal fibers in the original space; (B) QA mapping of the vertical fibers in the original space; (C) QA mapping of the horizontal fibers in the transformed space; and (D) QA mapping of the vertical fibers in the transformed space. In the original space, the QA values show a homogeneous pattern, since the fiber populations are uniform in the simulated space. In the transformed space, the QA mapping presents an inhomogeneous pattern, due to the diffeomorphic warping presented in Fig. 1(B). The

higher QA values represent higher packing of the fiber populations, whereas lower QA values represent lower packing.

The QA mappings of the horizontal and vertical fibers in the original space are shown in Fig. 3a and Fig. 3b, respectively. These QA mappings show homogeneous intensity, since the horizontal and vertical fibers have no deformation warping in the original space. The ratio between the accumulated QA of the horizontal and vertical fibers is 1.497, a value that reveals our simulation setting of the population ratio (3:2). The QA mapping of the horizontal and vertical fibers in the transformed space are shown in Fig. 3c and Fig. 3d, respectively. These QA mappings present inhomogeneous intensity due to the diffeomorphic warping, and the high intensity areas shown in Fig. 3c and Fig. 3d correspond to the areas with greater fiber packing shown in Fig. 1b. The ratio between the accumulated QA of the horizontal and vertical is 1.500, which is consistent with our simulation setting. This result shows that the accumulated QA obtained from the transformed SDFs can also reveal the fiber population ratio, even though the QA mapping in the transformed space presents an inhomogeneous pattern.

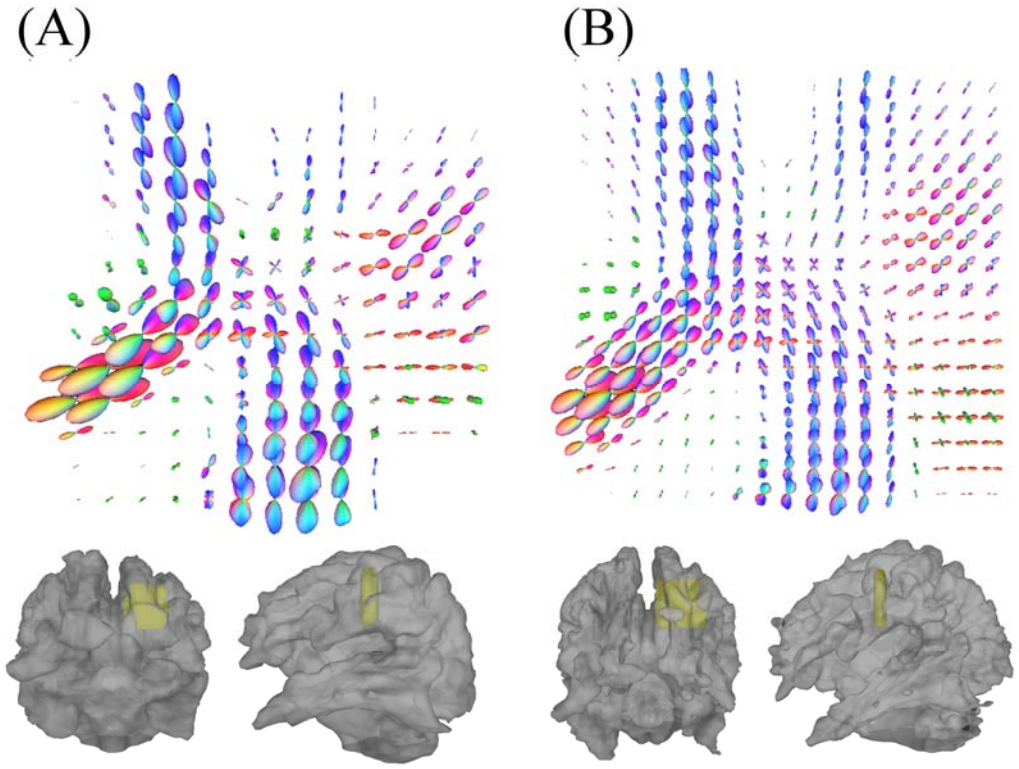

Fig. 4 The coronal slices of the spin distribution function (SDF) in the (A) original space and (B) ICBM-152 space. The slice focuses on the central semiovale, where the corticospinal tract, corpus callosum, and superior longitudinal fasciculus form a three-way crossing. The crossing fibers are readily discernable on both SDFs, and the resolve fiber

orientations are consistent with the anatomical structure.

In vivo study

To examine the performance of our method *in vivo*, we randomly selected one case from our normal volunteers and conducted qualitative comparison between the original and transformed SDFs, as shown in Fig. 4(a) and Fig. 4(b), respectively. The isotropic component of the SDF is removed to facilitate presentation, and directional colors are used to represent the orientations. The coronal slice was placed in the centrum semiovale, where corpus callosum, corticospinal tract, and superior longitudinal fasciculus form a three-way crossing region. As can be seen in the figure, the fiber orientations presented by the transformed SDFs show discernable crossing fiber orientations, and the fiber orientations follow the connection geometry of the fiber bundles. This suggests that the transformed SDF obtained from our q-space diffeomorphic reconstruction can resolve fiber orientations in the crossing regions.

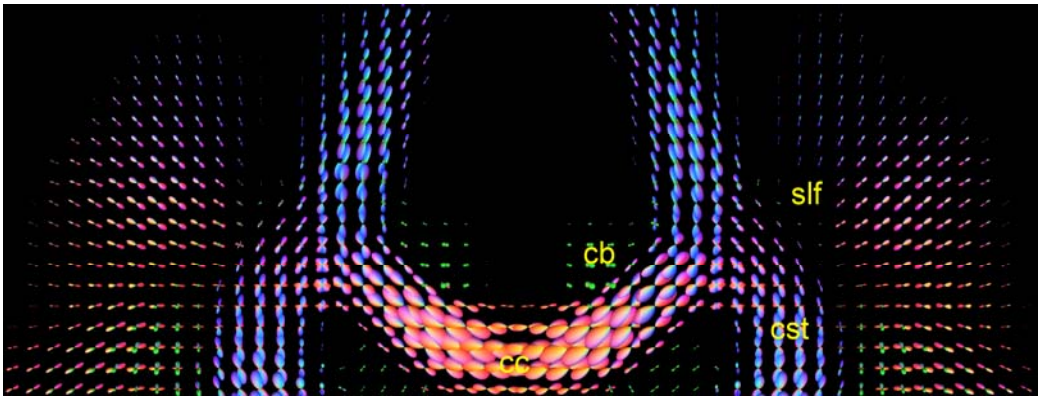

Fig. 5 The spin distribution function (SDF) of the NTU-90 brain atlas presented in the coronal view. The crossing fibers formed by the corpus callosum (cc) and corticospinal tract (cst) can be resolved by the SDFs. The anterior-posterior passing fibers can also be identified, such as the cingulum bundle (cb) and superior longitudinal fasciculus (slf). The corpus callosum fibers in the mid-sagittal region show larger SDFs due to their high packing density. The size gradually decreases as the fibers approach the gray matter, suggesting that the fibers fan out as they approach the cerebral cortex.

The SDFs of the NTU-90 atlas are shown in Fig. 5, where the coronal slice presents the body of the corpus callosum and centrum semiovale. The isotropic components of the SDFs are removed to present the anisotropic component, and the size is scaled according to the remaining magnitude of the SDF. As shown in the figure, the SDFs present the connections between the corpus callosum (cc) and cerebral cortex, and also the connection between the corticospinal tracts (cst) and the motor cortex. These two connections form a crossing region that is readily discernable by the SDFs. The anterior-posterior passing fibers can also be identified, including

the cingulum bundle (cb) and superior longitudinal fasciculus (slf). These SDFs demonstrate that our NTU-90 atlas can identify each individual fiber bundle in crossing regions and present their connection patterns. In addition to the fiber orientations, the magnitude of the SDF seems to reveal the compactness of the fiber bundles. Larger SDFs can be observed at the mid-sagittal portion of the corpus callosum fibers, which are known to be highly packed. The magnitude gradually decreases as fibers head toward the cerebral cortex, suggesting the spreading of the fibers as they approach the gray-white matter junction. This observation leads to speculation that the SDF could be used to reveal the number of axonal fibers; however, this claim requires examination in further studies.

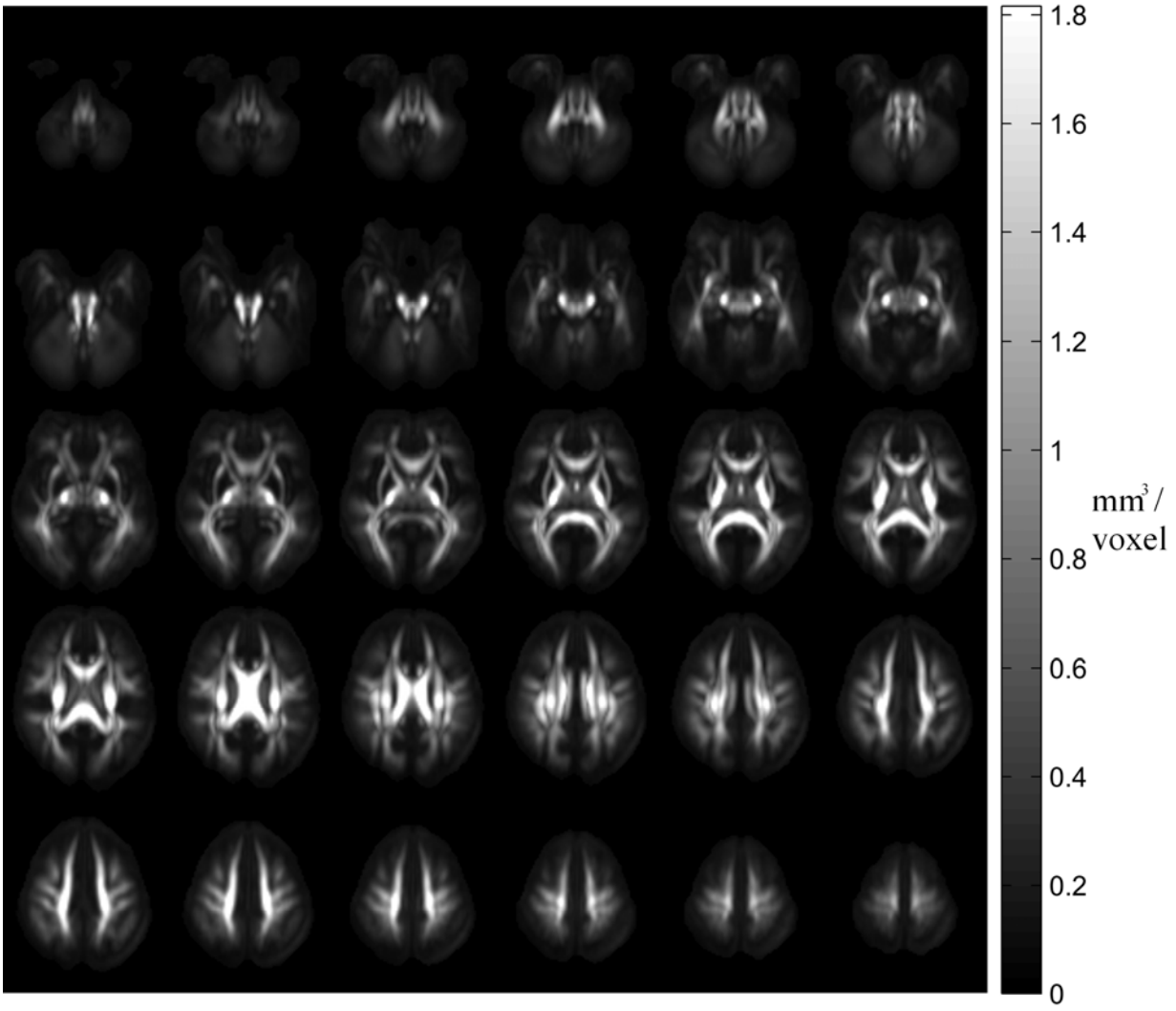

Fig. 6 The quantitative anisotropy (QA) mapping of the major fibers in the NTU-90 atlas. The major fiber is defined by the orientation of the maximum value on the obtained spin distribution function (SDF), so the major fiber represents the most prominent fiber population of a voxel. The QA mapping delineates white matter structures and reveals the amount of the diffusion spins in the major fiber population.

The QA of the major fibers of the NTU-90 atlas is shown in Fig. 6. The major fiber is defined by the maximum peak of the transformed SDF to present the most prominent fiber population in a given voxel. As shown in the figure, the QA mapping shows high intensity in regions having high compact fibers, such as the corpus callosum and internal capsule, whereas the gray matter regions have low intensity. This contrast pattern can be used to determine the termination location in fiber tracking.

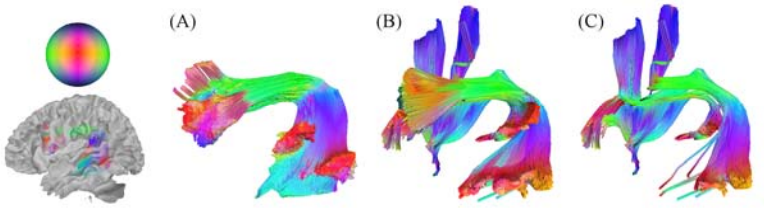

Fig. 7 (A) The tractography of the arcuate fasciculus generated from the NTU-90 atlas and (B) that generated from a DTI atlas. An identical tracking algorithm and parameters were used. The region of interest was placed at the supramarginal gyrus, and only the anterior-posterior fiber tracts were selected. The fiber tracts generated from the NTU-90 atlas present connections between the frontal and temporal lobes without visible deviation. In contrast, the fiber tracts generated from the DTI atlas suffer from obvious deviation, possibly due to the ambiguity of crossing fibers. The deviated fibers are presented in (C), showing false connections to corona radiata and inferior fronto-occipital fasciculus.

The tractography of the arcuate fasciculus fibers generated from NTU-90 and the DTI atlas are shown in Fig. 7. The fiber tracts of the arcuate fasciculus generated from the NTU-90 atlas present a curved bundle connecting frontal and temporal lobes without deviating to other tracts. In contrast, the fiber tracts generated from the DTI atlas show obvious upward and downward deviations near the prefrontal cortex. The deviated tracts were extracted using the fiber selection interface provided by DSI Studio and are shown in Fig. 7 (C); the fiber tracts deviate to the corona radiata and inferior fronto-occipital fasciculus via the crossing with the arcuate fasciculus. This underlines the limitation of DTI in resolving crossing fibers.

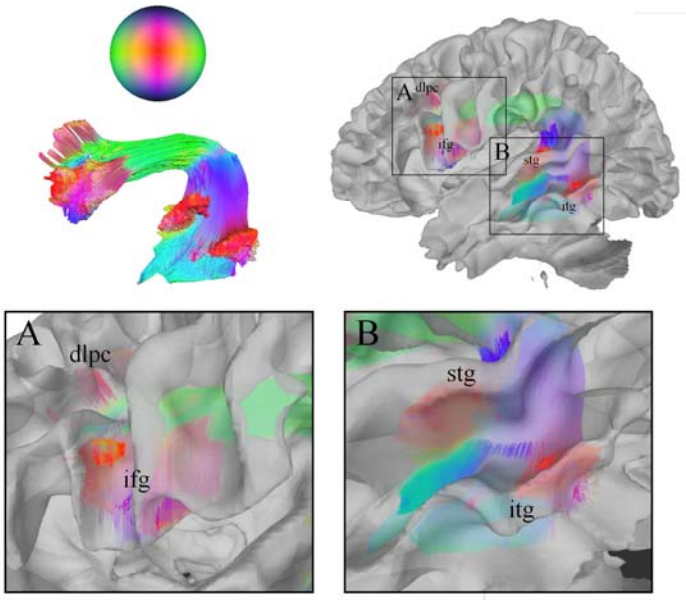

Fig. 8 Overlay of the cortical surface with the fiber tracts of the arcuate fasciculus generated from the NTU-90 atlas. The fiber tracts show definite termination near the dorsolateral prefrontal cortex (dlpc), inferior frontal gyrus (ifg), superior temporal gyrus (stg), and inferior temporal gyrus (itg). The cortical surface was independently generated from an externally supplied 1×1×1 mm resolution ICBM-152 white matter image. The tractography of the arcuate fasciculus shows continuous fiber pathways without interruption, and the cortical terminations match the anatomical locations of language processing. This demonstrates the potential application of the NTU-90 atlas to obtain fiber pathways and their functional localization in the cerebral cortex.

Fig. 8 shows the fiber tracts generated on the NTU-90 atlas and overlapped with the cortical surface. The cortical surface is rendered independently from an externally supplied 1×1×1 mm resolution ICBM-152 white matter image (Fonov et al., 2011). The inset figures further present the detail termination locations of the fiber tracts and their relative locations to the gyral folding near the dorsolateral prefrontal cortex (dlpc), inferior frontal gyrus (ifg), superior temporal gyrus (stg), and inferior temporal gyrus (itg); these regions are known to be related to language processing (Hickok and Poeppel, 2007). As shown in the figure, the tractography shows continuous fiber pathways without interruption, and the inset figures show that the locations of fiber terminations match the anatomical localization of the cortical regions related to language processing. This result suggests that fiber tracking can be applied to our atlas to obtain fiber pathways and localization of connected regions.

DISCUSSION

We present a high angular resolution brain atlas, NTU-90, which is constructed by applying our

q-space diffeomorphic reconstruction to 90 DSI datasets and averaging the transformed SDFs. The performance of our q-space diffeomorphic reconstruction method was examined by a simulation study. The simulation showed that the transformed SDF can preserve the principle fiber orientations, and the resolved fiber orientations can be used in fiber tracking to generate fiber tracts and to reveal the connection pattern in the transformed space. The accumulated QA obtained from the transformed SDFs can reveal the ratio of the fiber populations, even though the QA mapping presents an inhomogeneous pattern due to the diffeomorphic warping.

In addition to the simulation study, the performance of our q-space diffeomorphic reconstruction method was qualitatively examined on an *in vivo* dataset. The *in vivo* study demonstrates that the SDF can be transformed to the ICBM-152 space, and the peak orientations of the transformed SDFs are consistent with the anatomical structures. We also demonstrate that the averaged SDFs in the NTU-90 atlas can resolve crossing fibers and that the magnitude can reflect the packing density of the fiber bundles. The QA mapping of the major fiber in the NTU-90 atlas delineates the white matter structure, which can be used to define the terminations of fiber bundles. Further tractography results of the arcuate fasciculus showed continuous fiber pathways and definite cortical terminations related to language processing.

Our NTU-90 atlas offers some unique features that may worth noting. First, it is able to resolve crossing fibers and to support fiber tracking in fiber crossing regions. This feature can solve the crossing fiber problem of the DTI atlas and may have potential applications in brain connectome research. Second, the SDF of the NTU-90 atlas can reflect the variation of the relative fiber population, and the larger SDF can be observed in regions with high packing of fibers. This feature may be further exploited to quantify the brain connections. In addition to the features of our NTU-90 atlas, the q-space diffeomorphic reconstruction method proposed in this study also has several unique features. First, although not fully demonstrated in this study, the q-space diffeomorphic reconstruction method is readily applicable to a wide range of diffusion sampling schemes, including single-shell (also known as the high angular resolution diffusion imaging, HARDI), multiple-shell, and grid sampling scheme (also known as the DSI acquisition). This enables future studies to make use of either grid sampling or multiple shell sampling schemes. Second, the q-space diffeomorphic reconstruction method can be applied to any spatial transformation method that satisfies diffeomorphism, including rigid body transformation, affine transformation, and nonlinear transformations. As a result, our q-space reconstruction method is equally applicable to methods performing registration using diffusion MRI (Chiang et al., 2008; Leemans et al., 2006; Van Hecke et al., 2007) or using structure MRI. To obtain the transformed SDF, our method needs only the transformation functions defined by those methods and thus

opens up opportunities to incorporate their registration ability. Third, the transformed SDF obtained by our q-space diffeomorphic reconstruction is a spin quantity measurement, which is readily addable. In contrast, probabilistic measurements or fractional values such as diffusion ODF or FOD contain no spin density information, and direct addition of these measurements implicitly assumes that the spin density is uniform among subjects. Using these measurements to construct an atlas may require extra steps to consider the spin quantity difference between subjects. One may also note that DTI does not have spin density information, either. This is obvious in the first step of the tensor calculation, where the diffusion weighted signal is divided by the b0 signal, i.e. S(b)/S(0). This division cancels out the spin density, and the diffusion tensor estimated is also a probabilistic measurement based on Gaussian distribution, as pointed out by Basser (2002).

There are several limitations in our q-space diffeomorphic reconstruction. First, diffeomorphic mapping requires that the mapping function have an inverse function, and that the inverse function be differentiable. In practice, the existence of an inverse function implies that the subject and the template should have a one-to-one structure mapping, which may not be universally applicable. For example, subjects having pathological changes due to tumor or hematoma may not be eligible for diffeomorphic reconstruction, since it does not fulfill the one-to-one requirement. The second limitation is inherited from the GQI reconstruction, which requires additional spin density information to quantify the amount of diffusion spin. Alternatively, the b0 images can also be used as the spin density map if the T2 shine through effect is corrected.

The brain atlas constructed in this study also has limitations. First, all volunteers were recruited locally. This subject pool has a biased spectrum of age and may not fully represent the general population. Applying this atlas to a group study may require consideration of this limitation. Second, prominent distortion in the frontal base can be observed in our acquired diffusion images, and this distortion is also visible in our NTU-90 atlas. This susceptibility-induced distortion is due to the long EPI read-out, and it can be corrected by acquiring additional field maps (Hsu et al., 2009) or by using a higher acceleration factor in parallel imaging. In this study, we did not employ any of the above methods to minimize the distortion because the applicable field mapping techniques and parallel imaging with an acceleration factor of 4 were not readily available during the years of data collection. Hypothetically, the measured displacements could be combined with the displacement computed from the SPM spatial normalization and incorporated into the q-space diffeomorphic reconstruction. Third, the diffusion acquisition we used has a relatively low spatial resolution (3 mm isotropic resolution) in comparison to the

resolution of the ICBM-152 template (1 mm isotropic resolution). The inadequate resolution may result in inaccurate mapping of the fine structures, and a better spatial resolution setting is needed to construct a high definition brain atlas. Fourth, we use b0 image as the spin density mapping to calculate the SDF, an approach that is not an accurate way to measure the spin density because we did not correct the T_2 shine through effect of the b0 images. An atlas that uses accurate spin density calibration is needed in future studies. Lastly, we did not evaluate the registration accuracy of the spatial normalization in SPM. By comparing with SPM, Klein et al. have reported that there are several spatial mapping methods that achieve better brain registration (Klein et al., 2009). Further improvement of the template should be attainable if a better method is used in a future study.

ACKNOWLEDGMENTS

The work is supported in part by the National Science Council, Taiwan (NSC99-2321-B-002-037 and NSC99-3112-B-002-030).

REFERENCES

Alexander, A.L., Hasan, K.M., Lazar, M., Tsuruda, J.S., Parker, D.L., 2001. Analysis of partial volume effects in diffusion-tensor MRI. Magn Reson Med 45, 770-780.

Alexander, D.C., Barker, G.J., Arridge, S.R., 2002. Detection and modeling of non-Gaussian apparent diffusion coefficient profiles in human brain data. Magn Reson Med 48, 331-340.

Ardekani, S., Sinha, U., 2006. Statistical representation of mean diffusivity and fractional anisotropy brain maps of normal subjects. J Magn Reson Imaging 24, 1243-1251.

Barrick, T.R., Clark, C.A., 2004. Singularities in diffusion tensor fields and their relevance in white matter fiber tractography. Neuroimage 22, 481-491.

Basser, P.J., 2002. Relationships between diffusion tensor and q-space MRI. Magn Reson Med 47, 392-397.

Basser, P.J., Mattiello, J., LeBihan, D., 1994. Estimation of the effective self-diffusion tensor from the NMR spin echo. J Magn Reson B 103, 247-254.

Basser, P.J., Pajevic, S., Pierpaoli, C., Duda, J., Aldroubi, A., 2000. In vivo fiber tractography using DT-MRI data. Magn Reson Med 44, 625-632.

Basser, P.J., Pierpaoli, C., 1996. Microstructural and physiological features of tissues elucidated by quantitative-diffusion-tensor MRI. J Magn Reson B 111, 209-219.

Bhagat, Y.A., Emery, D.J., Naik, S., Yeo, T., Beaulieu, C., 2007. Comparison of generalized autocalibrating partially parallel acquisitions and modified sensitivity encoding for diffusion tensor imaging. AJNR Am J Neuroradiol 28, 293-298.

Callaghan, P.T., 1993. Principles of Nuclear Magnetic Resonance Microscopy.

Chiang, M.C., Leow, A.D., Klunder, A.D., Dutton, R.A., Barysheva, M., Rose, S.E., McMahon, K.L., de Zubicaray, G.I., Toga, A.W., Thompson, P.M., 2008. Fluid registration of diffusion tensor images using information theory. IEEE Trans Med Imaging 27, 442-456.

Conturo, T.E., Lori, N.F., Cull, T.S., Akbudak, E., Snyder, A.Z., Shimony, J.S., McKinstry, R.C., Burton, H., Raichle, M.E., 1999. Tracking neuronal fiber pathways in the living human brain. Proc Natl Acad Sci U S A 96, 10422-10427.

Fonov, V., Evans, A.C., Botteron, K., Almli, C.R., McKinstry, R.C., Collins, D.L., 2011. Unbiased average age-appropriate atlases for pediatric studies. Neuroimage 54, 313-327.

Fritzsche, K.H., Laun, F.B., Meinzer, H.P., Stieltjes, B., 2010. Opportunities and pitfalls in the quantification of fiber integrity: What can we gain from Q-ball imaging? Neuroimage.

Goodlett, C., Davis, B., Jean, R., Gilmore, J., Gerig, G., 2006. Improved correspondence for DTI population studies via unbiased atlas building. Med Image Comput Comput Assist Interv Int Conf Med Image Comput Comput Assist Interv 9, 260-267.

Gudbjartsson, H., Patz, S., 1995. The Rician distribution of noisy MRI data. Magn Reson Med 34, 910-914.

Hickok, G., Poeppel, D., 2007. The cortical organization of speech processing. Nat Rev Neurosci 8, 393-402.
Hong, X., Arlinghaus, L.R., Anderson, A.W., 2009. Spatial normalization of the fiber orientation distribution based on high angular resolution diffusion imaging data. Magn Reson Med.
Hsu, Y.C., Hsu, C.H., Tseng, W.Y., 2009. Correction for susceptibility-induced distortion in echo-planar imaging using field maps and model-based point spread function. IEEE Trans Med Imaging 28, 1850-1857.
Jones, D.K., Griffin, L.D., Alexander, D.C., Catani, M., Horsfield, M.A., Howard, R., Williams, S.C., 2002. Spatial normalization and averaging of diffusion tensor MRI data sets. Neuroimage 17, 592-617.
Klein, A., Andersson, J., Ardekani, B.A., Ashburner, J., Avants, B., Chiang, M.C., Christensen, G.E., Collins, D.L., Gee, J., Hellier, P., Song, J.H., Jenkinson, M., Lepage, C., Rueckert, D., Thompson, P., Vercauteren, T., Woods, R.P., Mann, J.J., Parsey, R.V., 2009. Evaluation of 14 nonlinear deformation algorithms applied to human brain MRI registration. Neuroimage 46, 786-802.
Kuo, L.W., Chen, J.H., Wedeen, V.J., Tseng, W.Y., 2008. Optimization of diffusion spectrum imaging and q-ball imaging on clinical MRI system. Neuroimage 41, 7-18.
Leemans, A., Sijbers, J., De Backer, S., Vandervliet, E., Parizel, P., 2006. Multiscale white matter fiber tract coregistration: a new feature-based approach to align diffusion tensor data. Magn Reson Med 55, 1414-1423.
Merboldt, K.D., Hanicke, W., Bruhn, H., Gyngell, M.L., Frahm, J., 1992. Diffusion imaging of the human brain in vivo using high-speed STEAM MRI. Magn Reson Med 23, 179-192.
Mori, S., Crain, B.J., Chacko, V.P., van Zijl, P.C., 1999. Three-dimensional tracking of axonal projections in the brain by magnetic resonance imaging. Ann Neurol 45, 265-269.
Mori, S., Oishi, K., Jiang, H., Jiang, L., Li, X., Akhter, K., Hua, K., Faria, A.V., Mahmood, A., Woods, R., Toga, A.W., Pike, G.B., Neto, P.R., Evans, A., Zhang, J., Huang, H., Miller, M.I., van Zijl, P., Mazziotta, J., 2008. Stereotaxic white matter atlas based on diffusion tensor imaging in an ICBM template. Neuroimage 40, 570-582.
Moseley, M.E., de Crespigny, A.J., Roberts, T.P., Kozniewska, E., Kucharczyk, J., 1993. Early detection of regional cerebral ischemia using high-speed MRI. Stroke 24, I60-65.
Muller, H.P., Unrath, A., Ludolph, A.C., Kassubek, J., 2007. Preservation of diffusion tensor properties during spatial normalization by use of tensor imaging and fibre tracking on a normal brain database. Phys Med Biol 52, N99-109.
Oouchi, H., Yamada, K., Sakai, K., Kizu, O., Kubota, T., Ito, H., Nishimura, T., 2007. Diffusion anisotropy measurement of brain white matter is affected by voxel size: underestimation occurs in areas with crossing fibers. AJNR Am J Neuroradiol 28, 1102-1106.

Park, H.J., Kubicki, M., Shenton, M.E., Guimond, A., McCarley, R.W., Maier, S.E., Kikinis, R., Jolesz, F.A., Westin, C.F., 2003. Spatial normalization of diffusion tensor MRI using multiple channels. Neuroimage 20, 1995-2009.

Peng, H., Orlichenko, A., Dawe, R.J., Agam, G., Zhang, S., Arfanakis, K., 2009. Development of a human brain diffusion tensor template. Neuroimage 46, 967-980.

Pierpaoli, C., Basser, P.J., 1996. Toward a quantitative assessment of diffusion anisotropy. Magn Reson Med 36, 893-906.

Pierpaoli, C., Jezzard, P., Basser, P.J., Barnett, A., Di Chiro, G., 1996. Diffusion tensor MR imaging of the human brain. Radiology 201, 637-648.

Reese, T.G., Benner, T., Wang, R., Feinberg, D.A., Wedeen, V.J., 2009. Halving imaging time of whole brain diffusion spectrum imaging and diffusion tractography using simultaneous image refocusing in EPI. J Magn Reson Imaging 29, 517-522.

Reese, T.G., Heid, O., Weisskoff, R.M., Wedeen, V.J., 2003. Reduction of eddy-current-induced distortion in diffusion MRI using a twice-refocused spin echo. Magn Reson Med 49, 177-182.

Tournier, J.D., Calamante, F., Gadian, D.G., Connelly, A., 2004. Direct estimation of the fiber orientation density function from diffusion-weighted MRI data using spherical deconvolution. Neuroimage 23, 1176-1185.

Tuch, D.S., 2004. Q-ball imaging. Magn Reson Med 52, 1358-1372.

Tuch, D.S., Reese, T.G., Wiegell, M.R., Makris, N., Belliveau, J.W., Wedeen, V.J., 2002. High angular resolution diffusion imaging reveals intravoxel white matter fiber heterogeneity. Magn Reson Med 48, 577-582.

Van Hecke, W., Leemans, A., D'Agostino, E., De Backer, S., Vandervliet, E., Parizel, P.M., Sijbers, J., 2007. Nonrigid coregistration of diffusion tensor images using a viscous fluid model and mutual information. IEEE Trans Med Imaging 26, 1598-1612.

Van Hecke, W., Sijbers, J., D'Agostino, E., Maes, F., De Backer, S., Vandervliet, E., Parizel, P.M., Leemans, A., 2008. On the construction of an inter-subject diffusion tensor magnetic resonance atlas of the healthy human brain. Neuroimage 43, 69-80.

Wedeen, V.J., Hagmann, P., Tseng, W.Y., Reese, T.G., Weisskoff, R.M., 2005. Mapping complex tissue architecture with diffusion spectrum magnetic resonance imaging. Magn Reson Med 54, 1377-1386.

Wedeen, V.J., Wang, R.P., Schmahmann, J.D., Benner, T., Tseng, W.Y., Dai, G., Pandya, D.N., Hagmann, P., D'Arceuil, H., de Crespigny, A.J., 2008. Diffusion spectrum magnetic resonance imaging (DSI) tractography of crossing fibers. Neuroimage 41, 1267-1277.

Williams, R., 2010. The human connectome: just another 'ome? Lancet Neurol 9, 238-239.

Xu, D., Mori, S., Shen, D., van Zijl, P.C., Davatzikos, C., 2003. Spatial normalization of diffusion tensor fields. Magn Reson Med 50, 175-182.

Yap, P.-T., Chen, Y., An, H., Gilmore, J.H., Lin, W., Shen, D., 2010. Hierachical Spherical Harmonics Based Deformable HARDI Registration. Lecture Notes in Computer Science 6326.
Yap, P.T., Chen, Y., An, H., Yang, Y., Gilmore, J.H., Lin, W., Shen, D., 2011. SPHERE: SPherical Harmonic Elastic REgistration of HARDI data. Neuroimage 55, 545-556.
Yeh, F.C., Wedeen, V.J., Tseng, W.Y., 2010. Generalized q-sampling imaging. IEEE Trans Med Imaging 29, 1626-1635.
Zhan, W., Yang, Y., 2006. How accurately can the diffusion profiles indicate multiple fiber orientations? A study on general fiber crossings in diffusion MRI. Journal of Magnetic Resonance 183, 193-202.
Zhang, H., Yushkevich, P.A., Alexander, D.C., Gee, J.C., 2006. Deformable registration of diffusion tensor MR images with explicit orientation optimization. Med Image Anal 10, 764-785.
Zhang, S., Peng, H., Dawe, R.J., Arfanakis, K., 2011. Enhanced ICBM diffusion tensor template of the human brain. Neuroimage 54, 974-984.